Intermetallic Compounds Hot Paper

International Edition: DOI: 10.1002/anie.201807934
German Edition: DOI: 10.1002/ange.201807934

Discovery of Cu_3Pb

*Alexandra D. Tamerius, Samantha M. Clarke, Mingqiang Gu, James P. S. Walsh, Marco Esters, Yue Meng, Christopher H. Hendon, James M. Rondinelli, Steven D. Jacobsen, and Danna E. Freedman**

Abstract: *Materials discovery enables both realization and understanding of new, exotic, physical phenomena. An emerging approach to the discovery of novel phases is high-pressure synthesis within diamond anvil cells, thereby enabling in situ monitoring of phase formation. Now, the discovery via high-pressure synthesis of the first intermetallic compound in the Cu-Pb system, Cu_3Pb is reported. Cu_3Pb is notably the first structurally characterized mid- to late-first-row transition-metal plumbide. The structure of Cu_3Pb can be envisioned as a direct mixture of the two elemental lattices. From this new framework, we gain insight into the structure as a function of pressure and hypothesize that the high-pressure polymorph of lead is a possible prerequisite for the formation of Cu_3Pb. Crucially, electronic structure computations reveal band crossings near the Fermi level, suggesting that chemically doped Cu_3Pb could be a topologically nontrivial material.*

The discovery of new intermetallic compounds lies at the intersection of inorganic chemistry, materials science, and condensed matter physics. Of particular import for materials discovery are binary intermetallic compounds exhibiting emergent phenomena, key examples include Weyl fermions in Mn_3Sn[1] and topological superconductivity in Au_2Pb.[2] Through the exploration of binary phase space where no compounds have been reported, we aim to discover new materials, elucidate their properties, and thereby improve our understanding of emergent phenomena. Our exploration is inspired by the idea that interacting an element with a large degree of spin–orbit coupling (SOC) with an element bearing either conduction electrons or spin-polarized electrons may catalyze the discovery of new exotic materials. Harnessing SOC from heavy elements can engender a wide variety of properties ranging from permanent magnetism to topologically protected states.[3–5] Based on the design criteria of employing SOC to impact physical properties of binary compounds, we sought to combine lead with copper. Lead offers tremendous SOC by virtue of its position on the periodic table. We selected copper, the canonical example of a conductive material, as a source of mobile electrons to probe the impact of SOC on electronic structure. Thus, the Cu-Pb system is promising for the isolation of new intermetallic compounds that exhibit emergent properties ranging from superconductivity to topologically nontrivial behavior.

Inspection of the thermodynamic phase diagram reveals the absence of thermodynamically stable Cu-Pb binary intermetallic compounds (Supporting Information, Figure S1).[6] To access a metastable phase, we can employ a variety of techniques that have demonstrated success within the solid-state synthesis field. Within the plethora of synthetic approaches, our vector of choice is high-pressure, high-temperature (high-*PT*) synthesis. Pressure alters the thermodynamics of a system, effectively adding a third axis to a binary temperature versus composition phase diagram. By applying high pressure, it is possible to create a phase that becomes thermodynamically stable at pressure yet is thermodynamically unstable under ambient conditions. Upon removal of pressure, the inherent kinetic stability of the newly created phase can in some cases enable the recovery of the metastable material.[7,8] Indeed, high-*PT* synthesis has led to the discovery of new metastable materials in numerous binary systems lacking thermodynamically stable binary compounds, such as Fe-Bi, Cu-Bi, Co-Bi.[9–13]

Herein, we report the discovery via high-*PT* synthesis of the first intermetallic compound in the Cu-Pb system, Cu_3Pb. Notably, Cu_3Pb is the first structurally characterized binary intermetallic compound of lead with any of the mid- to late-first-row transition metals (Cr–Zn).[14] We compare the crystal structure of Cu_3Pb to the elemental copper and lead structures and hypothesize that the high-pressure polymorph of lead is a possible prerequisite for the formation of Cu_3Pb. We also report electronic structure calculations of Cu_3Pb that

[*] A. D. Tamerius, Dr. J. P. S. Walsh, Prof. D. E. Freedman
Department of Chemistry, Northwestern University
Evanston, IL 60208 (USA)
E-mail: danna.freedman@northwestern.edu
Dr. S. M. Clarke
Physical and Life Sciences Directorate
Lawrence Livermore National Laboratory
Livermore, CA 94550 (USA)
Dr. M. Gu, Prof. J. M. Rondinelli
Department of Materials Science and Engineering
Northwestern University
Evanston, IL 60208 (USA)
Dr. M. Esters
Center for Materials Genomics, Duke University
Durham, NC 27708 (USA)
Prof. S. D. Jacobsen
Department of Earth and Planetary Sciences
Northwestern University
Evanston, IL 60208 (USA)
Prof. C. H. Hendon
Department of Chemistry and Biochemistry, University of Oregon
Eugene, OR 97403 (USA)
Dr. Y. Meng
HPCAT, Geophysical Laboratory, Carnegie Institute of Washington
Argonne, IL 60439 (USA)
Supporting information and the ORCID identification number(s) for the author(s) of this article can be found under: https://doi.org/10.1002/anie.201807934.

reveal potential for the realization of emergent properties within this phase.

To enable our exploration of the Cu–Pb phase space at high pressures and temperatures, we employed a laser-heated diamond anvil cell (LHDAC).[15] The transparency of diamond to a wide region of the electromagnetic spectrum enables us to monitor the reaction in situ with powder X-ray diffraction (PXRD) while heating with a near-IR laser, thereby monitoring the growth of new crystalline phases during the reaction. LHDACs can access a vast range of pressures extending beyond 100 GPa by exerting a force on a sample placed between two diamond anvils. Concurrently, LHDACs use a near-IR laser (FWHM ca. 40 μm) capable of heating samples to greater than 3000 K. For each experiment, we prepared a LHDAC with a mixture of elemental copper and lead prepared via arc-melting (Supporting Information, Figure S2). Laser-cut single-crystal MgO discs[16] placed around the sample thermally insulated the sample from the diamonds and served both as the pressure transmitting medium and as a pressure calibrant (Supporting Information, Figure S3).[17] PXRD data were collected at beamline 16-ID-B, HPCAT, Advanced Photon Source (APS, $\lambda = 0.406626$ Å, X-ray FWHM of 5–10 μm) during pressurization and heating, enabling us to observe the formation of new compounds in situ.[13]

To target new Cu-Pb binary intermetallic compounds, we explored pressures between 11–19 GPa. Elemental lead undergoes a phase transition from face-centered cubic (*fcc*) to hexagonal-close-packed (*hcp*) at approximately 13 GPa.[18–21] We hypothesized that this would be a promising pressure region for performing reactions as other systems exhibit higher reactivity in the region of a polymorphic elemental phase transition.[9,10] Prior to heating the arc-melted mixture of copper and lead at 15.7(2) GPa, the PXRD pattern consisted of peaks from Cu, Pb (*fcc*), Pb (*hcp*), and MgO. While heating up to approximately 850 K, we observed the anticipated phase transition from Pb (*fcc*) to Pb (*hcp*), consistent with previous reports.[16–19] Above approximately 950 K, we began to observe the growth of new peaks signaling the formation of a new phase. We held this temperature until the peaks were no longer growing in intensity (ca. 20 min). Then, we thermally quenched the sample by turning off the laser power supply. The PXRD pattern of the cooled sample consisted of peaks from Pb (*hcp*), MgO, Cu, and a new phase (Figure 1). Additional LHDAC reactions carried out at 16.4(3) GPa and 19.2(1) GPa with laser heating to maximum temperatures of approximately 1250 K and approximately 1300 K, respectively, resulted in the formation of the same new phase, illustrating wide phase stability (Supporting Information, Tables S2, S3, S6, S7). At 11 GPa, we did not observe the formation of Cu_3Pb even upon reaching the melting point of Pb (*fcc*) (ca. 1000 K). At 14 GPa and approximately 1300 K, we observed a minor peak that potentially corresponds to Cu_3Pb. However, we did not observe any significant formation of the new phase, thereby illustrating the lower end of the pressure stability region.

Approaching the structure solution of the new phase necessitated differentiating the peaks generated by the new phase from those of Pb (*hcp*), Cu, and MgO. We analyzed our

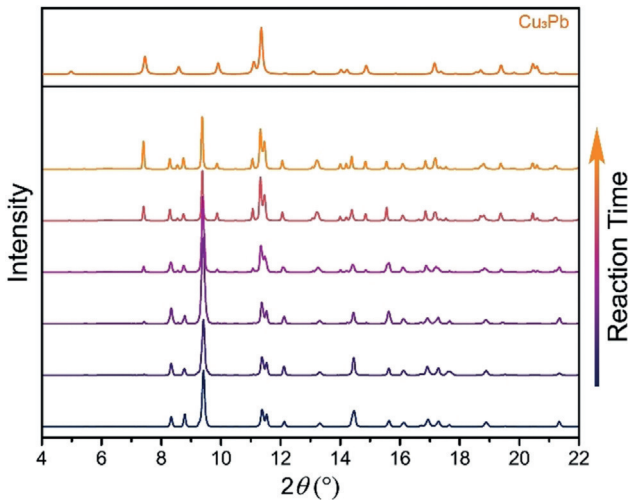

Figure 1. In situ PXRD data collected while heating a mixture of elemental copper and lead at 15.7(2) GPa ($\lambda = 0.406626$ Å). Each pattern has been background subtracted for clarity. The calculated pattern of Cu_3Pb from the Rietveld refined structure at 15.7(2) GPa is included for comparison (top).

data using the DIOPTAS software package.[22] First, we identified peaks that were unique to the new phase by observing their growth during heating (Figure 1). However, peak overlap between the new phase and the existing phases prevented a definitive structure solution. To deconvolute overlapping peaks, we examined the polycrystalline texture of each phase in the raw 2D diffraction images. By classification of the distinct polycrystalline textures in the raw 2D data, we were able to identify those peaks from the new phase that were obscured in the integrated powder pattern (Supporting Information, Figure S6). This procedure allowed us to index the new phase in the space group $P6_3/mmc$, with $a = 5.4361(2)$ Å and $c = 4.2011(3)$ Å at 15.7(2) GPa (Supporting Information, Figure S7) using TOPAS.[23]

Using a combination of reference structures and Rietveld refinement, we confirmed that the new phase was Cu_3Pb in the Ni_3Sn structure-type, and the first binary intermetallic compound in the Cu-Pb system (Supporting Information, Figure S7, Tables S1, S5).[24,25] The structure of Cu_3Pb can be envisioned as a distorted *hcp* lattice of Cu and Pb atoms, where the Cu atoms form 1D columns of face-sharing [Cu_6] octahedra running parallel to the *c*-axis (Supporting Information, Figure S8). The deviation of Cu_3Pb from a perfect *hcp* lattice with the same unit cell arises via a distortion of the Cu atoms in the *ab*-plane (Supporting Information, Table S5). In the Cu_3Pb structure, this distortion manifests itself as a contraction of the Cu–Cu distances in the 1D columns and the concomitant expansion of the Cu–Pb distances. The deviation of Cu_3Pb from a simple *hcp* lattice follows from the difference in the atomic radius of lead and copper and is in accordance with literature precedent for binary Ni_3Sn-type compounds with large differences in atomic radii.[26–28]

Consideration of the structure of Cu_3Pb is facilitated by inspection of the structures of the elemental precursors at high pressure. Note, for comparison, all distances discussed below are for structures obtained from the PXRD data

acquired at 15.7(2) GPa. Elemental lead forms a *hcp* lattice at approximately 13 GPa, while elemental copper remains in the *fcc* structure from ambient pressure up to at least 153 GPa.[18–21,29] We can describe Cu_3Pb as an amalgam of these two structures. Cu_3Pb features an expanded *hcp* sublattice of Pb atoms with [Cu_6] octahedra from the Cu (*fcc*) structure filling the interstitial space (Figure 2).

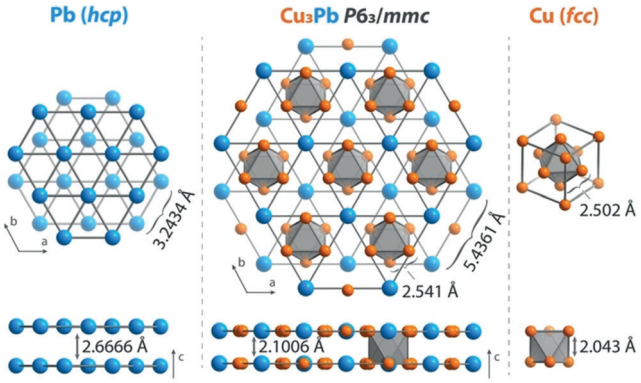

Figure 2. Depiction of the Cu_3Pb structure at 15.7(2) GPa as an ordered combination of the elemental structures. High-pressure Pb (*hcp*) and Cu (*fcc*) both at 15.7(2) GPa are depicted on the left and right, respectively. The Pb atoms are depicted as blue spheres and the Cu atoms as orange spheres.

Compared to the Pb (*hcp*) structure, the sublattice of Pb atoms in Cu_3Pb is expanded by approximately 2 Å along the *a*- and *b*-axes from 3.2434(1) Å to 5.4361(2) Å, and contracted by approximately 0.5 Å along the *c*-axis from 2.6666(2) Å to 2.1006(2) Å. The expansion of the lead lattice in the *ab*-plane creates suitable interstitial spaces for the [Cu_6] octahedra featured in the elemental Cu structure. The contraction of the lead lattice along the *c*-axis enables reasonable interlayer Cu–Cu distances. Indeed, the Cu–Cu distances in Cu_3Pb of 2.48(1) Å and 2.54(1) Å in and out of the *ab*-plane, respectively, are comparable to the 2.502(1) Å Cu–Cu distances in Cu (*fcc*). This suggests that Pb (*hcp*) may be distorting to accommodate [Cu_6] octahedra from elemental Cu (*fcc*) in the Cu_3Pb structure. Remarkably, we only observe significant formation of Cu_3Pb at least 1 GPa above the polymorphic phase transition from Pb (*fcc*) to Pb (*hcp*). Thus, we hypothesize that the formation of the Pb (*hcp*) lattice is an important prerequisite for the synthesis of Cu_3Pb, potentially templating intermetallic formation.

The shortest Pb–Pb distance, 3.7766(1) Å, in Cu_3Pb is 0.5 Å longer than the shortest contact in Pb (*hcp*) of 3.2434(1) Å. This difference suggests that the Pb–Pb interactions in the Cu_3Pb structure are weak in comparison to Pb (*hcp*). By halving the shortest interatomic distances in the elemental Cu and Pb (*hcp*) structures at 15.7(2) GPa, we can approximate the high-pressure atomic radii as 1.25 Å and 1.62 Å, respectively. In comparison to the sum of the high-pressure Cu and Pb atomic radii, 2.87 Å, the Cu–Pb distances in Cu_3Pb are at least 0.1 Å shorter: 2.72(1) Å and 2.708(3) Å. This suggests that there are Cu–Pb bonding interactions in Cu_3Pb at 15.7(2) GPa. The shortest Cu–Pb distance, 2.708-(3) Å, is out of the *ab*-plane, which indicates a preference for shorter and possibly stronger interlayer Cu–Pb interactions than intralayer interactions. This bonding analysis is supported by crystal orbital Hamiltonian populations (COHP) calculations discussed in the Supporting Information.

To assess whether Cu_3Pb could be recovered to ambient conditions, we incrementally decreased the pressure within the LHDAC while performing in situ PXRD experiments at room temperature (Supporting Information, Figure S9). Minutes after decompressing to ambient conditions, we observed peaks corresponding to Cu_3Pb in the diffraction patterns down to ambient pressure. This suggests that Cu_3Pb is pressure-quenchable within minutes of reaching ambient pressure (Supporting Information, Figure S10, Tables S4, S8, S9). By closely examining the decompression data, however, we noticed that the intensities of the Cu_3Pb peaks decrease during the experiment. Moreover, all attempts to isolate the high-pressure synthesized Cu_3Pb at ambient pressures thus far resulted in elemental Cu and Pb, suggesting that Cu_3Pb may not persist at ambient conditions, or that alternate conditions may be required to stabilize Cu_3Pb at ambient pressure. Future experiments will aim to stabilize Cu_3Pb to ambient conditions.

The crystal structure of Cu_3Pb gives rise to a fascinating electronic structure. In the similar compound, Mn_3Sn, which crystallizes in the same structure type as Cu_3Pb, the kagome nets of Mn atoms contribute to its exotic electronic properties.[1] Namely, the threefold symmetry and large SOC, contributed by the Sn atoms, facilitate odd numbers of Dirac cones in the band structure that are indicative of robust topological surface states.[1,3] These features in the band structure, when combined with broken time-reversal symmetry in the Mn kagome lattice, give rise to the first Weyl fermions observed in a strongly correlated material.[1] Although the distortion of the 6h Cu Wykoff position drastically distorts the kagome lattice of Cu atoms in Cu_3Pb, the hexagonal symmetry and large SOC present in Cu_3Pb are promising for promoting topologically nontrivial states.[1,3]

To better understand the electronic structure of Cu_3Pb, we performed density functional theory (DFT) calculations using a semilocal exchange-correlation functional (see the Supporting Information for more detail). Figure 3 shows the low

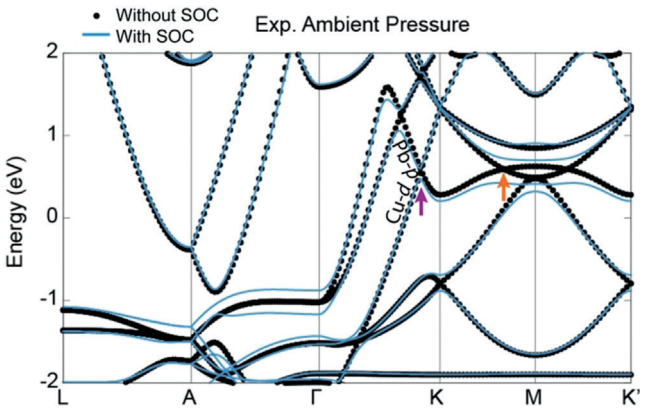

Figure 3. Electronic band structure for Cu_3Pb (experimental structure at ambient pressure) with (line) and without (dotted) spin–orbit coupling. The purple arrow shows a nodal point, and the orange arrow shows a nodal ring at about 0.5 eV. The Fermi level is set to 0 eV.

energy electronic structure of the experimental Cu_3Pb phase obtained at ambient pressure. The electronic states near the Fermi level arise from dispersive Pb 6p, Cu 3d, and 4s states, as is expected for an intermetallic phase derived from sd- and p-band metals. Unlike the analogous Mn_3Sn structure,[1] the Brillouin zone of Cu_3Pb is six-fold symmetric, that is, the neighboring M-points are equivalent, because the system is non-magnetic (time-reversal is present). Intriguingly, Cu_3Pb exhibits two types of band crossings that are observed approximately 0.5 eV above the Fermi level. Within the k_x–k_y plane, there are six nodal rings around the M-points (denoted by an orange arrow in Figure 3), which are gapped (by 0.4 eV) when SOC is considered. This level repulsion is similar to the nodal rings located about the K-point in Mn_3Sn. The Pb-p states and Cu-d states contribute to the bands near the nodal rings. The changes in the relative energies of these states shift the center of the nodal ring from the K-points to M-point in the Brillouin zone, compared to Mn_3Sn. The second crossing is located along the $\Gamma \rightarrow K$ path (purple arrow). The gap of this second crossing is much smaller (ca. 0.1 eV) when SOC is included. This point corresponds to a one-dimensional Dirac point, rather than a nodal ring. Furthermore, SOC results in band inversion about this point. Note that the band dispersions about the M-point are affected by local changes to the structure; for example, for a fully relaxed structure under zero pressure, the Cu–Pb bond lengths elongate, decreasing the orbital overlap. The separation of the bands at the M-points then increases from the reduced dispersion such that the nodal ring near the M-point vanishes, even without SOC included (Supporting Information, Figure S14). These results demonstrate the sensitivity of the electronic and quantum states near the M-point in Cu_3Pb to external pressure. The sensitivity to pressure in combination with the two types of band crossings just above the Fermi level suggest that anomalous Hall conductivity could be observed if in future experiments if we introduce a small chemical pressure to shift the Fermi level closer to the band crossing points.

The foregoing results illustrate the discovery via in situ high-pressure synthesis of Cu_3Pb, the first copper–lead binary compound. We describe the Cu_3Pb structure as a simultaneous incorporation of the elemental structures, which illuminates a hypothesis for the formation of Cu_3Pb at about 16 GPa. The band structure exhibits two types of band crossings that are sensitive to small structural changes. Thus, Cu_3Pb could be an exciting target for future doping studies that could likewise lead to isolation of doped Cu_3Pb at ambient conditions. Future work in this system will focus on obtaining chemically doped Cu_3Pb at ambient pressures and probing its electronic properties.

Acknowledgements

We thank Ryan Klein, Dr. Lei Sun and Dr. Alison Altman for helpful discussions, Dr. Curtis Kenney-Benson and Rich Ferry for technical support, and Chung-Jui Yu for assistance with the table of contents graphic. The collaborative project between D.E.F. and S.D.J. is supported by Northwestern University (NU) through the Innovative Initiatives Incubator (I3). Experimental work is supported by the AFOSR (FA95501410358) and (FA95501710247). S.M.C. acknowledges support from the NSF GRFP (DGE-1324585) and a P.E.O. Scholar Award. Part of this work was performed under the auspices of the U.S. Department of Energy by Lawrence Livermore National Security, LLC, under Contract DE-AC52-07NA27344. S.D.J. acknowledges support from NSF (DMR-1508577) and the Carnegie/DOE Alliance Center (CDAC) for providing beamtime at HPCAT. HPCAT operations are supported by DOE-NNSA under award no. DE-NA0001974, with partial instrumentation funding by NSF. Y.M. acknowledges the support of DOE-BES/DMSE under award no. DEFG02-99ER45775. M.G. was supported by the U.S. DOE, Office of Basic Energy Sciences, under grant no. DE-SC0012375 and J.M.R. was supported by the Alfred P. Sloan Foundation fellowship (Grant No. FG-2016-6469). All calculations were performed on the Extreme Science and Engineering Discovery Environment (XSEDE), which is supported by the NSF under grant no. ACI-1548562. This work made use of the EPIC facility of the NUANCE Center, and IMSERC, which is supported by Soft and Hybrid Nanotechnology Experimental (SHyNE) Resource (NSF ECCS-1542205); the MRSEC program (NSF DMR-1121262) at the Materials Research Center; the International Institute for Nanotechnology (IIN); the Keck Foundation; and the State of Illinois, through the IIN.

Conflict of interest

The authors declare no conflict of interest.

Keywords: diamond anvil cells · high-pressure synthesis · intermetallic compounds · metastable materials · X-ray crystallography

How to cite: *Angew. Chem. Int. Ed.* **2018**, *57*, 12809–12813
Angew. Chem. **2018**, *130*, 12991–12995

[1] K. Kuroda, T. Tomita, M.-T. Suzuki, C. Bareille, A. A. Nugroho, P. Goswami, M. Ochi, M. Ikhlas, M. Nakayama, S. Akebi, R. Noguchi, R. Ishii, N. Inami, K. Ono, H. Kumigashira, A. Varykhalov, T. Muro, T. Koretsune, R. Arita, S. Shin, T. Kondo, S. Nakatsuji, *Nat. Mater.* **2017**, *16*, 1090–1095.
[2] L. M. Schoop, L. S. Xie, R. Chen, Q. D. Gibson, S. H. Lapidus, I. Kimchi, M. Hirschberger, N. Haldoaarchchige, M. N. Ali, C. A. Belvin, T. Liang, J. B. Neaton, N. P. Ong, A. Vishwanath, R. J. Cava, *Phys. Rev. B* **2015**, *91*, 214517.
[3] R. J. Cava, H. Ji, M. K. Fuccillo, Q. D. Gibson, Y. S. Hor, *J. Mater. Chem. C* **2013**, *1*, 3176–3189.
[4] R. W. McCallum, L. H. Lewis, R. Skomski, M. J. Kramer, I. E. Anderson, *Annu. Rev. Mater. Res.* **2014**, *44*, 451–477.
[5] "Non-Centrosymmetric Superconductors": *Lecture Notes in Physics*, *Vol. 847* (Eds.: E. Bauer, M. Sigrist), Springer, Heidelberg, **2012**.
[6] H. Okamoto, *J. Phase Equilib.* **1993**, *14*, 649–650.
[7] L. Zhang, Y. Wang, J. Lv, Y. Ma, *Nat. Rev. Mater.* **2017**, *2*, 17005.
[8] E. Stavrou, Y. Yao, A. F. Goncharov, S. S. Lobanov, J. M. Zaug, H. Liu, E. Greenburg, V. B. Prakapenka, *Phys. Rev. Lett.* **2018**, *120*, 96001.

[9] J. P. S. Walsh, S. M. Clarke, Y. Meng, S. D. Jacobsen, D. E. Freedman, *ACS Cent. Sci.* **2016**, *2*, 867 – 871.
[10] S. M. Clarke, J. P. S. Walsh, M. Amsler, C. D. Malliakas, T. Yu, S. Goedecker, Y. Wang, C. Wolverton, D. E. Freedman, *Angew. Chem. Int. Ed.* **2016**, *55*, 13446 – 13449; *Angew. Chem.* **2016**, *128*, 13644 – 13647.
[11] S. M. Clarke, M. Amsler, J. P. S. Walsh, T. Yu, Y. Wang, Y. Meng, S. D. Jacobsen, C. Wolverton, D. E. Freedman, *Chem. Mater.* **2017**, *29*, 5276 – 5285.
[12] K. Guo, L. Akselrud, M. Bobnar, U. Burkhardt, M. Schmidt, J.-T. Zhao, U. Schwarz, Y. Grin, *Angew. Chem. Int. Ed.* **2017**, *56*, 5620; *Angew. Chem.* **2017**, *129*, 5712.
[13] U. Schwarz, S. Tencé, O. Janson, C. Koz, C. Krellner, U. Burkhardt, H. Rosner, F. Steglich, Y. Grin, *Angew. Chem. Int. Ed.* **2013**, *52*, 9853 – 9857; *Angew. Chem.* **2013**, *125*, 10038 – 10042.
[14] There is one report of NiPb crystallizing in the NiAs structure type that is formed by simultaneous vaporization. R. R. Ritti, J. Diximier, A. Guinier, *C. R. Seances Acad. Sci. Ser. A* **1968**, *266*, 565 – 567.
[15] Y. Meng, R. Hrubiak, E. Rod, R. Boehler, G. Shen, *Rev. Sci. Instrum.* **2015**, *86*, 072201.
[16] R. Hrubiak, S. Sinogeikin, E. Rod, G. Shen, *Rev. Sci. Instrum.* **2015**, *86*, 072202.
[17] S. Speziale, C.-S. Zha, T. S. Duffy, R. J. Hemley, H.-K. Mao, *J. Geophys. Res.: Solid Earth* **2001**, *106*, 515 – 528.
[18] H. K. Mao, Y. Wu, J. F. Shu, J. Z. Hu, R. J. Hemley, D. E. Cox, *Solid State Commun.* **1990**, *74*, 1027 – 1029.
[19] T. Takahashi, H. K. Mao, W. A. Bassett, *Science* **1969**, *165*, 1352 – 1353.
[20] A. Kuznetsov, V. Dmitriev, L. Dubrovinsky, V. Prakapenka, H.-P. Weber, *Solid State Commun.* **2002**, *122*, 125 – 127.
[21] A. Dewaele, M. Mezouar, N. Guignot, P. Loubeyre, *Phys. Rev. B* **2007**, *76*, 144106.
[22] C. Prescher, V. B. Prakapenka, *High Pressure Res.* **2015**, *35*, 223 – 230.
[23] A. A. Coelho, TOPAS Academic: General Profile and Structure Analysis Software for Powder Diffraction Data; Bruker AXS: Karlsruhe, Germany, **2007**.
[24] Inorganic Crystal Structure Database (ICSD) Web, Version 3.5.0, FIZ Karlsruhe, Germany, **2017**.
[25] A. L. Lyubimtseva, A. I. Baranov, A. Fischer, L. Kloo, B. A. Popovkin, *J. Alloys Compd.* **2002**, *340*, 167 – 172.
[26] E. E. Havinga, *J. Less-Common Met.* **1975**, *41*, 241 – 254.
[27] J. H. N. Van Vucht, K. H. J. Buschow, *J. Less-Common Met.* **1965**, *10*, 98 – 107.
[28] *Handbook of Chemistry and Physics 98th ed.* [Online] (Ed.: J. R. Rumble), CRC Press/Taylor & Francis, Boca Raton FL, **2018**.
[29] A. Dewaele, P. Loubeyre, M. Mezouar, *Phys. Rev. B* **2004**, *70*, 094112.

Manuscript received: July 11, 2018
Version of record online: September 4, 2018

